Journal of Molecular Catalysis A: Chemical 344 (2011) 138–144

Contents lists available at ScienceDirect

Journal of Molecular Catalysis A: Chemical

journal homepage: www.elsevier.com/locate/molcata

Synthesis, characterization and photocatalytic activity of $AgBr/H_2WO_4$ composite photocatalyst

Jing Cao*, Bangde Luo, Haili Lin, Shifu Chen*

College of Chemistry and Materials Science, Huaibei Normal University, 100 Dongshan Road, Anhui, Huaibei 235000, China

ARTICLE INFO

Article history:
Received 27 February 2011
Received in revised form 15 May 2011
Accepted 16 May 2011
Available online 25 May 2011

Keywords:
$AgBr/H_2WO_4$
Deposition–precipitation method
Surface plasmon
Reaction mechanism

ABSTRACT

A new composite photocatalyst $AgBr/H_2WO_4$ was prepared by loading H_2WO_4 on AgBr substrate via deposition–precipitation method and characterized by X-ray diffraction (XRD), scanning electron microscopy (SEM), energy-dispersive spectroscopy (EDS) and UV–vis diffuse reflectance spectroscopy (DRS). Photocatalytic degradation of methyl orange (MO) and rhodamine B (RhB) was carried out to evaluate the photocatalytic activity of $AgBr/H_2WO_4$ under visible-light irradiation ($\lambda > 420$ nm). The photocatalytic results show that the $AgBr/H_2WO_4$ composite could degrade MO and RhB efficiently and had much higher photocatalytic activity than AgBr or H_2WO_4. X-ray photoelectron spectroscopy (XPS) suggests that $AgBr/H_2WO_4$ transformed to be $Ag/AgBr/H_2WO_4$ system while remained good photocatalytic activity after 5 times of cycle experiments. In addition, the quenching effect was examined in the photocatalytic reaction process of MO and RhB, respectively. Active h^+, Br^0 and the resulting $^\bullet O_2^-$ played the major roles for the dye degradation while $^\bullet OH$ was verified to be insignificant. The high photocatalytic activity and good stability are closely related to the efficient electron–hole pairs separation derived from the matching band potentials between AgBr and H_2WO_4, as well as the surface plasmon resonance of Ag nanoparticles formed on AgBr particles during the photocatalytic reaction process.

1. Introduction

To resolve energy shortage and environmental pollution problem, semiconductor photocatalysis is highly expected to be an ideal "green" technology [1] for the conversion of solar energy and photo-oxidation of organic pollutants. However, the widely used photocatalyst TiO_2 (with large band gap of 3.2 eV) is limited to irradiation wavelengths in the UV range [2–4], which makes it necessary to develop efficient visible-light-driven photocatalysts to meet the requirements of future application. Consequently design of new photocatalysts has become an imperative topic in current photocatalysis research.

Silver halides (AgX, X = Cl, Br, I) are important photosensitive semiconductors (SCs) extensively employed in photography field. Under light irradiation AgX can absorb photons to generate electrons and holes. Thus AgX can be used as potential photocatalysts. But the photoinduced electrons will combine with interstitial Ag^+ ions to form an Ag^0 cluster, which leads to the unwanted and uncontrolled photodecomposition of AgX. The instability of pure AgX is a main obstacle in practical photocatalytic application.

In recent years, a great number of attempts have been made by efficiently trapping photoinduced electrons, avoiding the reaction between electrons and Ag^+, to improve the photostability of AgX.

(1) *Ag/AgX system*. Ag nanoparticles (NPs) on the surface of AgX act as efficient electrons traps as well as plasmon under visible-light irradiation, such as Ag@AgBr [5–8], Ag@AgCl [9–13] and Ag@Ag(Br,I) [14].
(2) *AgX-based composite SCs*. In these cases, the conduction band (CB) bottom and the valence band (VB) top of SCs lie below the CB bottom and VB top of AgX, respectively. Hence the photoinduced electrons at the CB bottom of AgX can migrate to that of SCs and finally are trapped by O_2 molecules to form superoxide ions ($^\bullet O_2^-$) and other reactive oxygen species. This kind of composite photocatalytsts include $AgBr/TiO_2$ [15], AgI/TiO_2 [16], $H_2WO_4{\cdot}H_2O/AgCl$ [17], AgI/BiOI [18] and $AgBr/WO_3$ [19].
(3) *Ag/AgX-based composite photocatalysts*. For these specific systems, Ag NPs show efficient surface plasmon resonance (SPR) in visible region and trap photoinduced electrons to prevent them from combining with Ag^+. In addition, if the AgX and SCs have matching band potentials, electrons and holes can be effectively separated and further improve the activity of catalysts. At present, majority of the substrates are inert, such as SiO_2 [20], TiO_2 [21–26], Al_2O_3 [27,28], Al-MCM-41 [29,30], Y-zeolite [31], Fe_3O_4 [32] and ZnO [33]. However, only a little active substrates,

* Corresponding authors. Tel.: +86 561 3806611; fax: +86 561 3803141.
E-mail addresses: caojing@mail.ipc.ac.cn (J. Cao), chshifu@chnu.edu.cn (S. Chen).

1381-1169/$ – see front matter © 2011 Elsevier B.V. All rights reserved.
doi:10.1016/j.molcata.2011.05.012

such as $WO_3 \cdot H_2O$ [34], Bi_2WO_6 [35,36] and $Ag_8W_4O_{16}$ [37] can play the above duplicate roles, which display higher activity and better stability under visible-light irradiation. Therefore, among the above strategies, it will be a promising way to utilize AgX as photosensitive components in photocatalytic field.

In the present study, a novel $AgBr/H_2WO_4$ was constructed and synthesized by a facile deposition–precipitation method. The CB bottom and the VB top of H_2WO_4 lie below the CB bottom and VB top of AgBr, respectively, which will result in the highly efficient separation of photoinduced electrons and holes. Moreover, $AgBr/H_2WO_4$ can easily transform to be $Ag/AgBr/H_2WO_4$ system in the early stage of the photocatalytic reaction, which will exert the role of Ag NPs. Methyl orange (MO) and rhodamine B (RhB) were used as model pollutants to evaluate photocatalytic activity of the $AgBr/H_2WO_4$ composites under visible-light irradiation ($\lambda > 420$ nm). The stability of the photocatalyst was also investigated via the repetition tests. Moreover, various scavengers were introduced to the photocatalytic reaction system to explore the roles of different reactive species and the reaction mechanism.

2. Experimental

2.1. Chemicals and materials

All reagents were of analytical purity and were used without further purification. Silver nitrate ($AgNO_3$), sodium bromide (NaBr), sodium tungstate dihydrate ($Na_2WO_4 \cdot 2H_2O$), ammonia solution, methyl orange (MO), rhodamine B (RhB), absolute ethanol, terephthalic acid (TA), benzoquinone (BQ), isopropanol (IPA), potassium iodide (KI), sodium hydroxide (NaOH) and nitric acid (HNO_3) were obtained from Sinopharm Chemical Reagent Co., Ltd. Deionized water was used throughout this study.

2.2. Preparation of $AgBr/H_2WO_4$ photocatalyst

The $AgBr/H_2WO_4$ was synthesized by deposition–precipitation method under red light. 6.79 g of $AgNO_3$ was dissolved in 35 mL ammonia solution and 4.12 g of NaBr was dissolved in deionized water in advance. Then NaBr solution was dropped into $AgNO_3$ solution with stirring. Subsequently, the mixture was vigorously stirred for 5 h at room temperature, and then yellow AgBr precipitate was obtained. 2.64 g of $Na_2WO_4 \cdot 2H_2O$ was dissolved in ethanol–water solution (1:2, v/v). The as-prepared AgBr dispersion was sonicated for 30 min before $Na_2WO_4 \cdot 2H_2O$ solution was added. After the pH of above suspension was adjusted to 2.0 with dilute HNO_3 solution, the reaction mixture was subsequently stirred for 10 h at 60 °C. Finally, yellow $AgBr/H_2WO_4$ precipitate was collected, washed with deionized water for 3 times, and dried at 65 °C for 24 h. Yellow $AgBr/H_2WO_4$ catalyst with theoretical Ag/W molar ratio of 1:0.20 was obtained.

2.3. Characterization of $AgBr/H_2WO_4$ photocatalyst

The powder X-ray diffraction (XRD) analysis of the as-prepared catalyst was carried out at room temperature with a Bruker D8 Advance X-diffractometer using Cu Kα radiation ($\lambda = 1.5406$ Å), operated at 40 kV and 40 mA, and a scanning speed of 10°/min. Scanning electron microscopy (SEM) measurements were recorded on a JEOL JSM-6610LV at scanning voltage of 30 kV. X-ray photoelectron spectroscopy (XPS) measurements were performed on a Thermo ESCALAB 250 with Al Kα (1486.6 eV) line at 150 W. To compensate for surface charges effects, binding energies were calibrated using the C1s hydrocarbon peak at 284.80 eV. Oxford instruments INCA X-act energy-dispersive spectroscopy (EDS) was employed to determine the final actual Ag/W molar ratio in the composite. The UV–vis diffuse reflectance spectra (DRS) were obtained by a Pgeneral TU-1901 UV-VIS spectrophotometer equipped with an integrating sphere assembly. The analysis range was from 300 to 800 nm, and $BaSO_4$ was used as a reflectance standard.

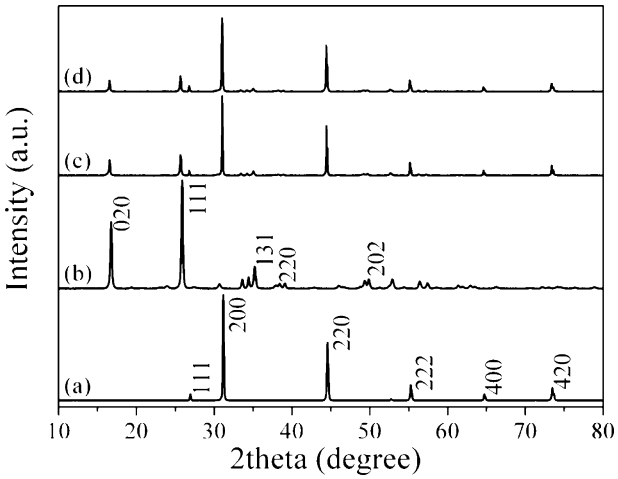

Fig. 1. XRD patterns of (a) AgBr, (b) H_2WO_4, (c) fresh $AgBr/H_2WO_4$ and (d) used $AgBr/H_2WO_4$.

2.4. Photocatalytic activities test

The photocatalytic degradation of MO and RhB were adopted to evaluate the photocatalytic activity of $AgBr/H_2WO_4$ in a photoreaction apparatus [38] under visible-light irradiation ($\lambda > 420$ nm). A 500 W Xe lamp (Institute of Electric Light Source, Beijing) was used as the light source with a 420 nm cutoff filter (Instrument Company of Nantong, China) to provide visible-light irradiation. In each experiment, 0.1 g photocatalyst was added into 50 mL of dye solution (10 mg/L). Prior to illumination, the suspension was magnetically stirred in the dark for 30 min to reach adsorption–desorption equilibrium of dye on catalyst surfaces. At every irradiation time intervals of 10 min, 5 mL of the suspension was collected, then centrifuged (4000 rpm, 30 min) to remove the photocatalyst particles. The catalyst-free dye solution was analyzed with a 722 s spectrophotometer (Shanghai Precision and Scientific Instrument Company, China). The concentration of dye was determined from its maximum absorption at a wavelength of 464 nm for MO and 554 nm for RhB with deionized water as a reference sample.

3. Results and discussion

3.1. XRD and XPS analyses

Fig. 1 shows the XRD patterns of the as-prepared samples. It is observed that AgBr (Fig. 1a) was face-centered cubic AgBr structure (JCPDS NO. 06-0438) while H_2WO_4 (Fig. 1b) was orthorhombic phase (JCPDS NO. 18-1418). In addition, the $AgBr/H_2WO_4$ composite (Fig. 1c) exhibited a coexistence of both AgBr and H_2WO_4 phases. The average crystalline sizes of AgBr and H_2WO_4 in the $AgBr/H_2WO_4$ composites were calculated to be 76.9 and 48.4 nm according to the Scherrer formula [39], respectively. Compared with the fresh $AgBr/H_2WO_4$, the used $AgBr/H_2WO_4$ after 5 successive photo-oxidation experiments (Fig. 1d) displays almost the same diffraction peaks.

However, it is difficult to draw any conclusions concerning the existence of Ag in the used $AgBr/H_2WO_4$ (Fig. 1d) from the XRD data, due to the possible superposition of Ag and AgBr peaks at 38.11°, as

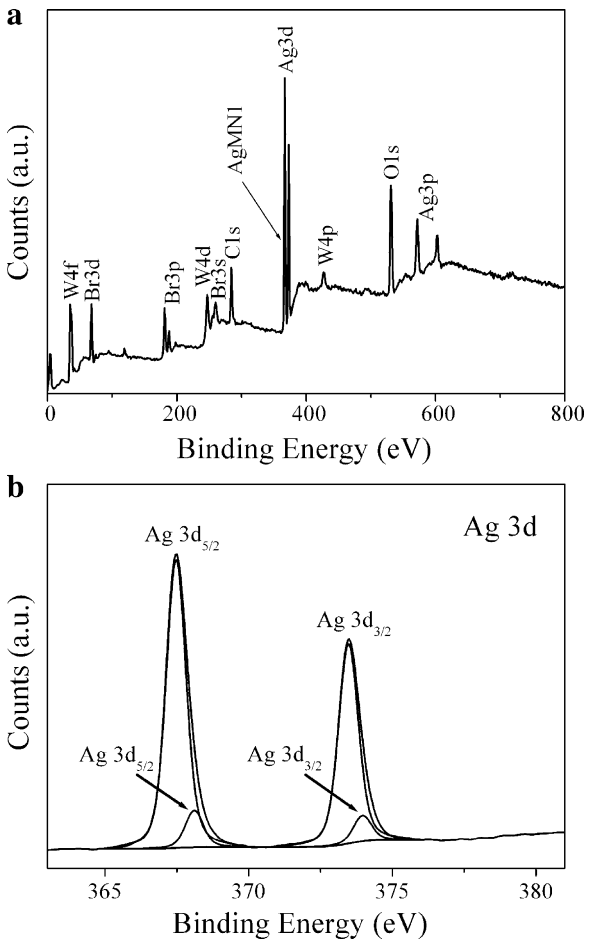

Fig. 2. (a) XPS survey spectrum of used $AgBr/H_2WO_4$ and (b) the corresponding high-resolution XPS spectrum of Ag 3d.

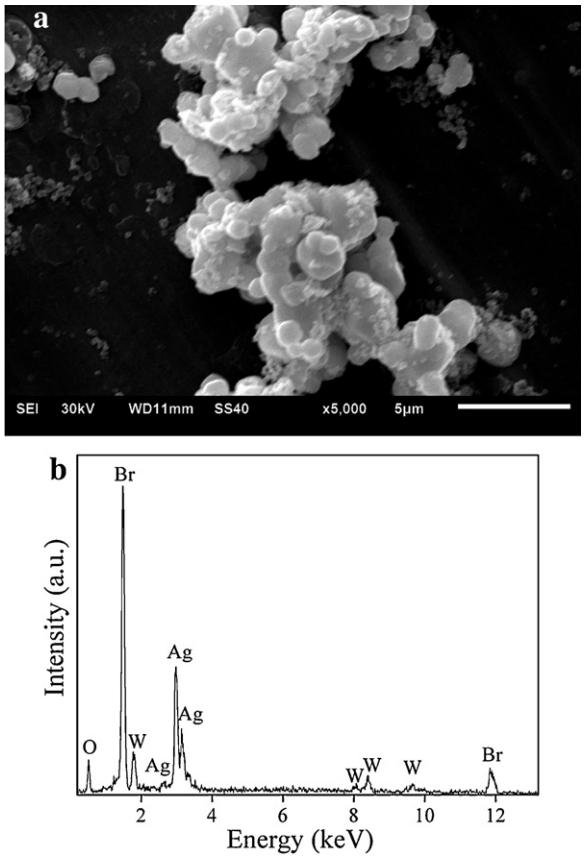

Fig. 3. (a) SEM images and (b) EDS of the as-prepared $AgBr/H_2WO_4$.

well as, Ag and H_2WO_4 peaks at 44.27°, respectively. Furthermore, the used catalyst became a little darker than the fresh catalyst. Therefore, the used $AgBr/H_2WO_4$ after 5 times cycle experiment was further characterized by XPS measurement and the results are shown in Fig. 2. Fig. 2a displays the XPS survey spectrum of the used $AgBr/H_2WO_4$ composites, which mainly exhibits the peaks of Ag, Br, W, O and C. The XPS peak for C 1s (284.8 eV) is ascribed to the adventitious hydrocarbon from the XPS instrument. A typical high-resolution XPS spectrum of Ag 3d is shown in Fig. 2b. The peaks at ~367 and ~373 eV are assigned to Ag $3d_{5/2}$ and Ag $3d_{3/2}$, respectively. The Ag $3d_{5/2}$ peak is further divided into two different peaks at 367.48 and 368.11 eV and the Ag $3d_{3/2}$ is also divided into two different peaks at 373.47 and 373.96 eV. According to Zhang et al. [40], the peaks at 368.11 and 373.96 eV can be attributed to metal Ag^0, whereas the peaks at 367.48 and 373.47 eV can be attributed to the Ag^+ of AgBr. The peaks at 368.11 and 373.96 eV to metal Ag^0 hence confirmed the existence of Ag^0 in the used $AgBr/H_2WO_4$ composites. From the XPS peak areas, the surface Ag^0 and Ag^+ contents are calculated to be 4.46 and 37.88 at.%. This result suggests that $AgBr/H_2WO_4$ has transformed to be $Ag/AgBr/H_2WO_4$ composite photocatalyst through light irradiation during the photocatalytic process without additional light reduction treatment before the photocatalysis.

3.2. SEM analysis

The SEM image of $AgBr/H_2WO_4$ (Fig. 3a) presents that H_2WO_4 particles with size of about 0.8 μm were mostly formed on the surface of AgBr particles that had irregular shapes with particle size of 1–4 μm. Besides, a fraction of H_2WO_4 particles were of self-nucleation. The corresponding EDS result (Fig. 3b) illustrates that the final actual Ag/W molar ratio in the $AgBr/H_2WO_4$ was 1:0.19, which was almost identical to the initial theoretical value (1:0.20).

3.3. DRS analysis

Fig. 4 shows the DRS of the AgBr, H_2WO_4, fresh $AgBr/H_2WO_4$ and the used $AgBr/H_2WO_4$ samples. As can be seen above, AgBr had an absorption edge at about 480 nm, while H_2WO_4 had broader absorption in the visible region with an absorption edge of around 530 nm. In addition, $AgBr/H_2WO_4$ composite displays clear optical

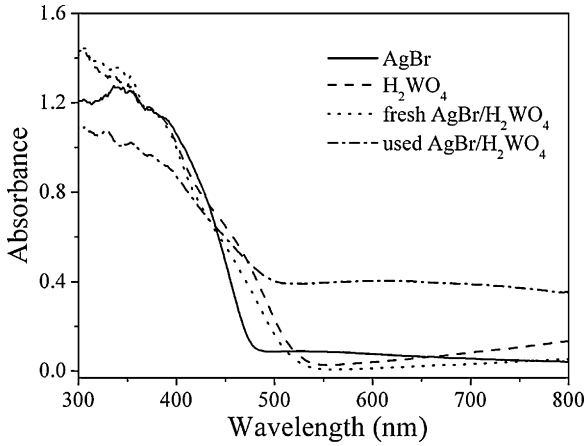

Fig. 4. DRS of AgBr, H_2WO_4, fresh $AgBr/H_2WO_4$ and used $AgBr/H_2WO_4$.

response in the visible region with an absorption edge of approximate 520 nm. Differently, the used $AgBr/H_2WO_4$ for 5 successive cycles had much stronger absorption in the visible region than that of AgBr, H_2WO_4 and fresh $AgBr/H_2WO_4$, which may result from the SPR of Ag NPs deposited on the AgBr particles [5–8,23,27,34]. Therefore, the DRS data also confirms the existence of Ag^0 in the used $AgBr/H_2WO_4$ composite.

The band gap energy of a semiconductor can be calculated by the following formula [41,42]:

$$\alpha h\nu = A(h\nu - E_g)^{n/2} \quad (1)$$

where α, h, ν, E_g and A are absorption coefficient, Planck constant, light frequency, band gap energy, and a constant, respectively. Among them, n is determined by the type of optical transition of a semiconductor (i.e., $n = 1$ for direct transition and $n = 4$ for indirect transition). For AgBr and H_2WO_4, the values of n are 4 and 1, respectively. Therefore, E_g of AgBr was determined from a plot of $(\alpha h\nu)^{1/2}$ versus energy ($h\nu$) (Fig. 5) and was found to be 2.49 eV. Accordingly, E_g of H_2WO_4 was elicited to be 2.47 eV according to a plot of $(\alpha h\nu)^2$ versus energy ($h\nu$) (Fig. 5).

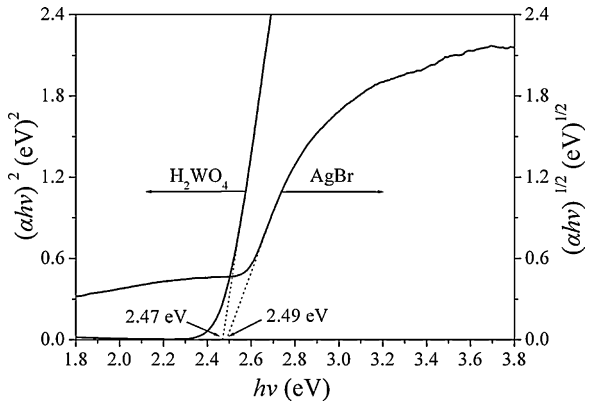

Fig. 5. Plot of $(\alpha h\nu)^{1/2}$ versus energy ($h\nu$) for the band gap energy of AgBr and the plot of $(\alpha h\nu)^2$ versus energy ($h\nu$) for the band gap energy of H_2WO_4.

3.4. Degradation of dyes using $AgBr/H_2WO_4$ photocatalyst

The photocatalytic activities of as-prepared samples were evaluated by the degradation of MO and RhB under visible-light irradiation. Fig. 6a displays the degradation of MO in aqueous dispersions by different photocatalysts with the same weight of active component. The degradation efficiency of MO was 95.10%, 53.10% and 0.50% for $AgBr/H_2WO_4$, AgBr and H_2WO_4 after irradiation for 60 min, respectively, which indicates that MO can be degraded more efficiently by $AgBr/H_2WO_4$ than single AgBr or H_2WO_4. In addition, the reference experiments including dark adsorption of MO by $AgBr/H_2WO_4$ and photolysis of MO without catalyst were also investigated. The results show that almost no MO degradation occurred in the dark or by photolysis. Moreover, the similar change tendency of degradation efficiency was also displayed in the process of RhB degradation (Fig. 6b) as that of MO degradation.

The catalyst's lifetime is an important parameter of the photocatalytic process, so it is essential to evaluate the stability of the catalyst for practical application. The repetition tests (Fig. 6c) reveal that the high photocatalytic performance of $AgBr/H_2WO_4$ for MO degradation was effectively maintained after 5 times cycle experiments except for 13.70% decrease in photocatalytic efficiency, which indicates that $AgBr/H_2WO_4$ has high stability under visible-light irradiation. Moreover, the stability of the $AgBr/H_2WO_4$ was also studied through the degradation of RhB (Fig. 6d) and further

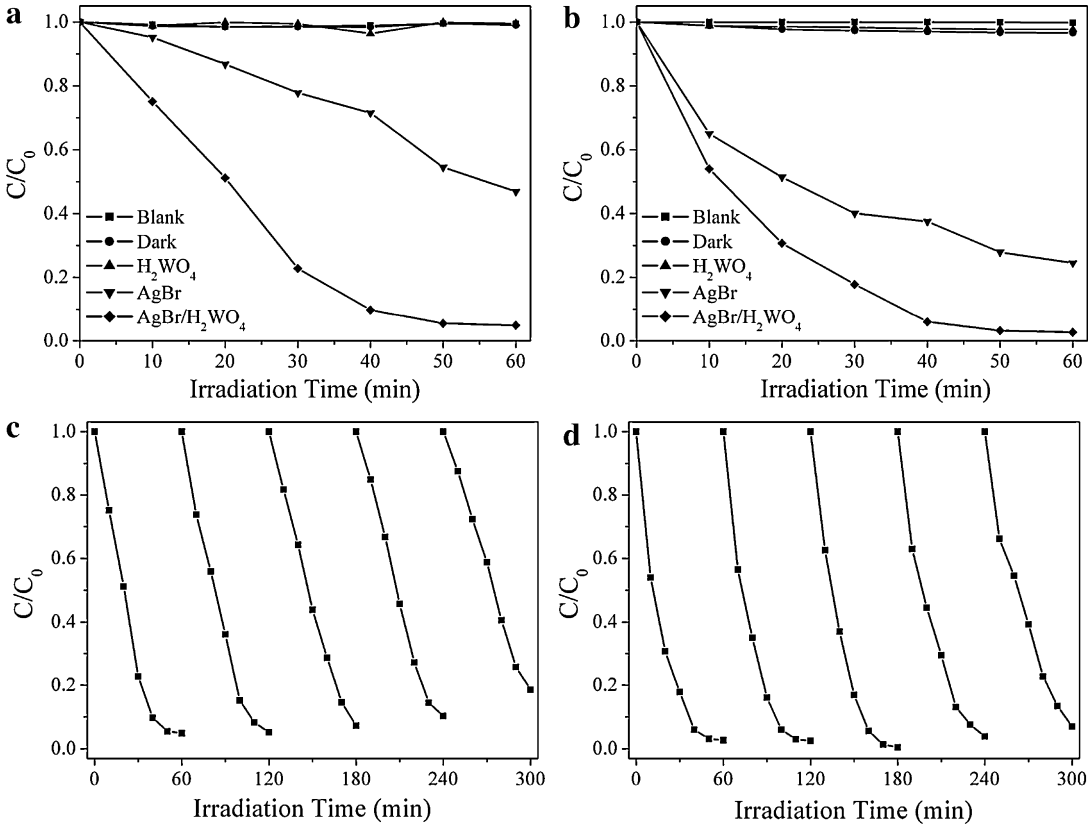

Fig. 6. (a) The degradation of MO by different photocatalysts with the same weight of each visible-light-active component (■) blank; (●) dark; (▲) 21.02 mg H_2WO_4; (▼)78.98 mg AgBr; (♦) 100.00 mg $AgBr/H_2WO_4$ photocatalyst containing 21.02 mg H_2WO_4 and 78.98 mg AgBr. (b) The degradation of RhB under the same condition as MO. (c) Cycling runs of $AgBr/H_2WO_4$ for the degradation of MO. (d) Cycling runs of $AgBr/H_2WO_4$ for the degradation of RhB.

Table 1
The effects of a series of scavengers on the k_{app} of MO and RhB degradation.

	Scavenger dosage	MO		RhB	
		k_{app} ($\times 10^{-2}$ min^{-1})	k_{app}/k_{app} (no quenching) (%)	k_{app} ($\times 10^{-2}$ min^{-1})	k_{app}/k_{app} (no quenching) (%)
No quenching	–	5.3	100	6.4	100
KI	0.1 mmol/L	4.4	83.0	0.3	4.70
IPA	0.1 mmol/L	5.1	96.2	6.2	96.9
BQ	0.1 mmol/L	1.5	28.3	4.2	65.6

confirms the good stability of $AgBr/H_2WO_4$. This result indicates that though $AgBr/H_2WO_4$ is not stable at the initial reaction process under visible-light irradiation, the formed $Ag/AgBr/H_2WO_4$ system can effectively retain its activity due to the efficient transfer of photoinduced electrons by Ag NPs.

3.5. Possible photocatalytic mechanism

3.5.1. Roles of reactive species

The excellent photocatalytic performance of the as-prepared $AgBr/H_2WO_4$ motivated us to further investigate the underlying photocatalytic mechanism. It is generally accepted that the dyes and organic pollutants can be photodegraded via photocatalytic oxidation (PCO) process. A large number of main reactive oxygen species (ROSs) involved in PCO process include h^+, •OH, and $•O_2^-$ [27,43,44].

Therefore, the effects of some scavengers on the degradation of MO (or RhB) were examined in attempt to elucidate the reaction mechanism. As an •OH scavenger, isopropanol (IPA) was added to the reaction system [36,45], and KI was introduced as the scavenger of h^+ and •OH [46,47]. Benzoquinone (BQ) was adopted to quench $•O_2^-$ [48,49]. As a consequence of quenching, PCO reaction will be partly suppressed and k_{app} (pseudo-first-order) is lowered. The more k_{app} is reduced by scavengers, the more important role the corresponding oxidizing species play in the PCO reaction [32].

Table 1 shows the effects of scavengers KI, IPA and BQ on the k_{app} of MO (or RhB) degradation. The roles of the counterpart species quenched can be calculated and indicated by k_{app}/k_{app} (no quenching) [50]. For MO degradation, the k_{app} of BQ and IPA quenching decreased to 28.3% and 96.2% of no quenching respectively, indicating that $•O_2^-$ has the main role in the process of MO oxidation, whereas •OH can be negligible in this process. Moreover, the k_{app} of KI quenching also decreased to 83.0%, suggesting that h^+ has minor effect for MO degradation after eliminating the role of •OH. Compared to MO, scavengers KI, IPA and BQ displayed different effects on RhB degradation. That is the main ROSs were h^+ and $•O_2^-$ for RhB degradation over $AgBr/H_2WO_4$. Huang et al. [5,34] and Geng et al. [6] have reported that Br^- can combine with an h^+ on AgBr to form Br^0, also as reactive radical species, further oxidizes dye molecules.

To further research whether •OH was formed after illuminated by visible-light irradiation, PL technique was employed to detect the •OH. The experimental process was carried out according to our previous report [19]. The PL emission spectra excited at 315 nm from TA solution suspension with $AgBr/H_2WO_4$ were measured every 20 min of illumination and the results are shown in Fig. 7. It can be seen that no PL signal at about 425 nm was observed, demonstrating that no •OH were formed in the PCO process, which was consistent with the IPA quenching results. In summary, the main reactive species involved in the degradation of MO (or RhB) are h^+, Br^0 and $•O_2^-$.

3.5.2. Band gap structures and possible degradation mechanism

The VB edge position of $AgBr/H_2WO_4$ composite was estimated in this study according to the concept of electronegativity. Herein, the electronegativity of an atom is the arithmetic mean of the atomic electron affinity and the first ionization energy. The valence band potential of a semiconductor at the point of zero charge can be calculated by the following empirical equation [51]:

$$E_{VB} = X - E^c + 0.5E_g \quad (2)$$

where E_{VB} is the VB edge potential, X is the electronegativity of the semiconductor, which is the geometric mean of the electronegativity of the constituent atoms, E^c is the energy of free electrons on the hydrogen scale (about 4.5 eV), E_g is the band gap energy of the semiconductor, and E_{CB} can be determined by $E_{CB} = E_{VB} - E_g$. The X values for AgBr and H_2WO_4 are 5.81 and 6.89 eV, and the E_{VB} of AgBr and H_2WO_4 were calculated to be 2.56 and 3.63 eV, respectively. Thus, the E_{CB} of AgBr and H_2WO_4 were estimated to be 0.07 and 1.16 eV, respectively.

On the base of band gap structure of as-prepared $AgBr/H_2WO_4$ and the effects of scavengers, possible pathway for the photocatalytic degradation of dyes with $AgBr/H_2WO_4$ photocatalyst was proposed as follows (Fig. 8): during the PCO process, the $AgBr/H_2WO_4$ system was transformed to be $Ag/AgBr/H_2WO_4$ system. Ag, AgBr and H_2WO_4 can be simultaneously excited to form electron–hole pairs under visible-light irradiation. Subsequently the photogenerated electrons transfer from the CB bottom of AgBr to that of H_2WO_4 or are trapped by Ag NPs formed on AgBr particles. At the same time photogenerated holes also move in the opposite direction from the VB top of H_2WO_4 to that of AgBr. Probably, electrons in the VB of AgBr could be excited up to a higher potential edge (−0.39 eV) under visible-light illumination with energy less than 2.95 eV ($\lambda > 420$ nm), and these electrons will be trapped by Ag NPs and further react with O_2 adsorbed on the surface of catalyst to generate reactive $•O_2^-$ [5–7,23,27,34] that induced the degradation of MO and RhB. However, the VB edge potential of H_2WO_4 (1.16 eV vs NHE) is more positive than E° ($O_2/•O_2^-$) (−0.046 eV vs NHE) [44,52], suggesting that the electrons at CB of H_2WO_4 cannot reduce O_2 to $•O_2^-$. Meanwhile, on the one hand, reactive holes at the VB of AgBr can oxidize Br^- ions to Br^0 atoms that are the reactive radical species and degrade MO and RhB [5–7,34]; on the other

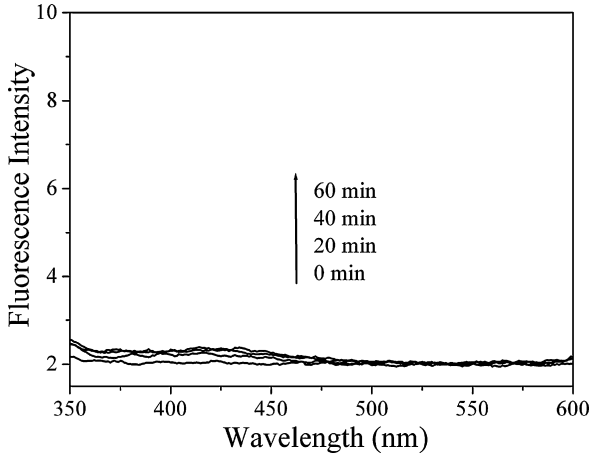

Fig. 7. •OH trapping PL spectra of $AgBr/H_2WO_4$ in TA solution under visible-light irradiation.

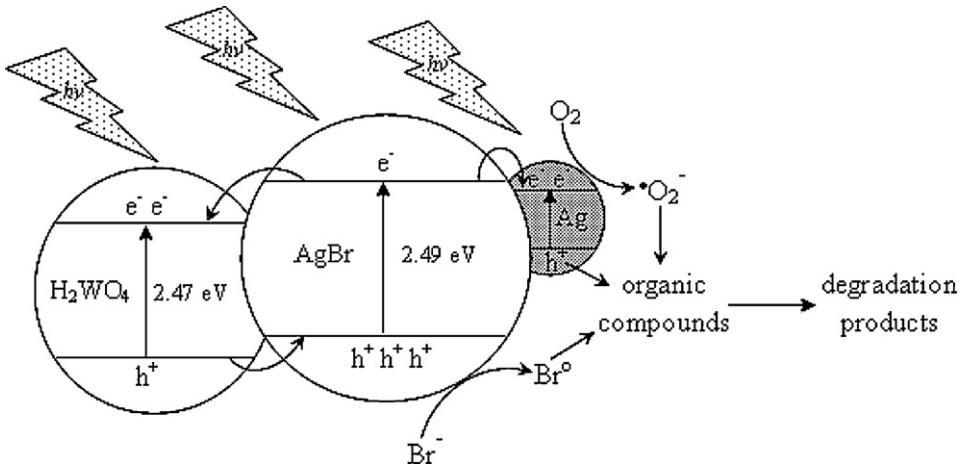

Fig. 8. Schematic diagram of electron–hole pairs separation and the possible reaction mechanism over $Ag/AgBr/H_2WO_4$ photocatalyst under visible-light irradiation.

hand, the holes generated on Ag NPs can also oxidize the MO and RhB directly [6,23,27]. In summary, MO and RhB were decomposed by $Ag/AgBr/H_2WO_4$ under visible-light irradiation through $^{\bullet}O_2^-$, Br^0 or direct h^+ oxidation pathway.

During the photocatalytic reaction process, recombination of the electrons and holes are efficiently prevented, and the reaction probability of electrons with Ag^+ is almost avoided. Consequently, the activity is kept at a high level, more importantly, the stability of AgBr is ensured at the same time.

4. Conclusions

The $AgBr/H_2WO_4$ was synthesized using a facile deposition–precipitation method. The as-prepared $AgBr/H_2WO_4$ exhibited excellent performance on the degradation of MO and RhB, and displayed much higher photocatalytic activity than single AgBr or H_2WO_4 under visible-light irradiation ($\lambda > 420$ nm). After 5 cycles of repetition tests, the degradation efficiency of MO or RhB still remained 81.40% and 93.00%, respectively. Photocatalytic mechanism investigations demonstrate that the degradation of MO and RhB over the as-prepared $AgBr/H_2WO_4$ under visible-light irradiation is mainly via $^{\bullet}O_2^-$ oxidation mechanism and the Br^0 (or direct h^+) oxidation pathway. It may be a promising efficient composite photocatalyst for environmental purification.

Acknowledgements

This work was financially supported by the Natural Science Foundation of China (No. 20973071), youth foundation of Huaibei Normal University (No. 700427) and Anhui Key Laboratory of Energetic Materials (No. KLEM2009013).

References

[1] M.R. Hoffmann, S.T. Martin, W. Choi, D.W. Bahnemann, Chem. Rev. 95 (1995) 69–96.
[2] V. Keller, P. Bernhardt, F. Garin, J. Catal. 215 (2003) 129–138.
[3] V. Iliev, D. Tomova, S. Rakovsky, A. Eliyas, G.L. Puma, J. Mol. Catal. A: Chem. 327 (2010) 51–57.
[4] X.Q. Zhu, J.L. Zhang, F. Chen, Chemosphere 78 (2010) 1350–1355.
[5] P. Wang, B.B. Huang, X.Y. Zhang, X.Y. Qin, H. Jin, Y. Dai, Z.Y. Wang, J.Y. Wei, J. Zhan, S.Y. Wang, J.P. Wang, M.H. Wangbo, Chem. Eur. J. 15 (2009) 1821–1824.
[6] L. Kuai, B.Y. Geng, X.T. Chen, Y.Y. Zhao, Y.C. Luo, Langmuir 26 (2010) 18723–18727.
[7] D.S. Wang, Y.D. Duan, Q.Z. Luo, X.Y. Li, L.L. Bao, Desalination 270 (2011) 174–180.
[8] Y.P. Bi, J.H. Ye, Chem. Eur. J. 16 (2010) 10311–10327.
[9] P. Wang, B.B. Huang, X.Y. Qin, X.Y. Zhang, Y. Dai, J.Y. Wei, M.H. Whangbo, Angew. Chem. Int. Ed. 47 (2008) 7931–7933.
[10] P. Wang, B.B. Huang, Z.Z. Lou, X.Y. Zhang, X.Y. Qin, Y. Dai, Z.K. Zheng, X.N. Wang, Chem. Eur. J. 16 (2010) 538–544.
[11] C.H. An, S. Peng, Y.G. Sun, Adv. Mater. 22 (2010) 2570–2574.
[12] H. Xu, H.M. Li, J.X. Xia, S. Yin, Z.J. Luo, L. Liu, L. Xu, ACS Appl. Mater. Interfaces 3 (2011) 22–29.
[13] Y.Y. Li, Y. Ding, J. Phys. Chem. C 114 (2010) 3175–3179.
[14] P. Wang, B.B. Huang, Q.Q. Zhang, X.Y. Zhang, X.Y. Qin, Y. Dai, J. Zhan, J.X. Yu, H.X. Liu, Z.Z. Lou, Chem. Eur. J. 16 (2010) 10042–10047.
[15] Y.Q. Lan, C. Hu, X.X. Hu, J.H. Qu, Appl. Catal. B: Environ. 73 (2007) 354–360.
[16] C. Hu, X.X. Hu, L.S. Wang, J.H. Qu, A.M. Wang, Environ. Sci. Technol. 40 (2006) 7903–7907.
[17] P. Wang, B.B. Huang, X.Y. Zhang, X.Y. Qin, Y. Dai, H. Jin, J.Y. Wei, M.H. Whangbo, Chem. Eur. J. 14 (2008) 10543–10546.
[18] H.F. Cheng, B.B. Huang, Y. Dai, X.Y. Qin, X.Y. Zhang, Langmuir 26 (2010) 6618–6624.
[19] J. Cao, B.D. Luo, H.L. Lin, S.F. Chen, J. Hazard. Mater. 190 (2011) 700–706.
[20] N. Kakuta, N. Goto, H. Ohkita, T. Mizushima, J. Phys. Chem. B 103 (1999) 5917–5919.
[21] Y.Y. Wen, H.M. Ding, Chin. J. Catal. 32 (2011) 36–45.
[22] M.R. Elahifard, S. Rahimnejad, S. Haghighi, M.R. Gholami, J. Am. Chem. Soc. 129 (2007) 9552–9553.
[23] C. Hu, Y.Q. Lan, J.H. Qu, X.X. Hu, A.M. Wang, J. Phys. Chem. B 110 (2006) 4066–4072.
[24] Y.Z. Li, H. Zhang, Z.M. Guo, J.J. Han, X.J. Zhao, Q.N. Zhao, S.J. Kim, Langmuir 24 (2008) 8351–8357.
[25] Y.J. Zang, R. Farnood, Appl. Catal. B: Environ. 79 (2008) 334–340.
[26] J.G. Yu, G.P. Dai, B.B. Huang, J. Phys. Chem. C 113 (2009) 16394–16401.
[27] X.F. Zhou, C. Hu, X.X. Hu, T.W. Peng, J.H. Qu, J. Phys. Chem. C 114 (2010) 2746–2750.
[28] C. Hu, T.W. Peng, X.X. Hu, Y.L. Nie, X.F. Zhou, J.H. Qu, H. He, J. Am. Chem. Soc. 132 (2010) 857–862.
[29] S. Rodrigues, S. Uma, I.N. Martyanov, K.J. Klabunde, J. Catal. 233 (2005) 405–410.
[30] A. Pourahmad, S. Sohrabnezhad, E. Kashefian, Spectrochim. Acta A: Mol. Biomol. Spectrosc. 77 (2010) 1108–1114.
[31] Y.J. Zang, R. Farnood, J. Currie, Chem. Eng. Sci. 64 (2009) 2881–2886.
[32] G.T. Li, K.H. Wong, X.W. Zhang, C. Hu, J.C. Yu, R.C.Y. Chan, P.K. Wong, Chemosphere 76 (2009) 1185–1191.
[33] Y.G. Xu, H. Xu, H.M. Li, J.X. Xia, C.T. Liu, L. Liu, J. Alloys Compd. 509 (2011) 3286–3292.
[34] P. Wang, B.B. Huang, X.Y. Qin, X.Y. Zhang, Y. Dai, M.H. Whangbo, Inorg. Chem. 48 (2009) 10697–10702.
[35] L.S. Zhang, K.H. Wong, Z.G. Chen, J.C. Yu, J.C. Zhao, C. Hu, C.Y. Chan, P.K. Wong, Appl. Catal. A: Gen. 363 (2009) 211–229.
[36] L.S. Zhang, K.H. Wong, H.Y. Yip, C. Hu, J.C. Yu, C.Y. Chan, P.K. Wong, Environ. Sci. Technol. 44 (2010) 1392–1398.
[37] X.F. Wang, S.F. Li, H.G. Yu, J.G. Yu, J. Mol. Catal. A: Chem. 334 (2011) 52–59.
[38] J. Cao, B.Y. Xu, B.D. Luo, H.L. Lin, S.F. Chen, Appl. Surf. Sci. 257 (2011) 7083–7089.
[39] M. Galceran, M.C. Pujol, C. Zaldo, F. Daz, M. Aguil, J. Phys. Chem. C 113 (2009) 15497–15506.
[40] H. Zhang, G. Wang, D. Chen, X.J. Lv, J.H. Li, Chem. Mater. 20 (2008) 6543–6549.
[41] M.A. Butler, J. Appl. Phys. 48 (1977) 1914–1920.
[42] J. Zeng, H. Wang, Y.C. Zhang, M.K. Zhu, H. Yang, J. Phys. Chem. C 111 (2007) 11879–11887.
[43] Y.Q. Yang, G.K. Zhang, S.J. Yu, X. Sheng, Chem. Eng. J. 162 (2010) 171–177.
[44] Y.Y. Li, J.S. Wang, H.C. Yao, L.Y. Dang, Z.J. Li, J. Mol. Catal. A: Chem. 334 (2011) 116–122.
[45] Y.X. Chen, S.Y. Yang, K. Wang, L.P. Lou, J. Photochem. Photobiol. A: Chem. 172 (2005) 47–54.
[46] S.H. Yoon, J.H. Lee, Environ. Sci. Technol. 39 (2005) 9695–9701.

[47] G.T. Li, J.H. Qu, X.W. Zhang, J.H. Liu, H.N. Liu, J. Mol. Catal. A: Chem. 259 (2006) 238–244.
[48] J. Bandara, J. Kiwi, New J. Chem. 23 (1999) 717–724.
[49] M.C. Yin, Z.S. Li, J.H. Kou, Z.G. Zou, Environ. Sci. Technol. 43 (2009) 8361–8366.
[50] X.W. Zhang, G.T. Li, Y.Z. Wang, J.H. Qu, J. Photochem. Photobiol. A: Chem. 184 (2006) 26–33.
[51] X. Zhang, L.Z. Zhang, T.F. Xie, D.J. Wang, J. Phys. Chem. C 113 (2009) 7371–7378.
[52] Z. Jiang, F. Yang, G.D. Yang, L. Kong, M.O. Jones, T.C. Xiao, P.P. Edwards, J. Photochem. Photobiol. A: Chem. 212 (2010) 8–13.